

Reconstructing the Vulcano Island evolution from 3D modeling of magnetic signatures

Rosalba Napoli and Gilda Currenti

Istituto Nazionale di Geofisica e Vulcanologia, Sezione di Catania, Osservatorio Etneo, Piazza Roma 2,
95125 Catania, Italy

Abstract

High-resolution ground and marine magnetic data are exploited for a detailed definition of a 3D model of the Vulcano Island volcanic complex. The resulting 3D magnetic imaging, obtained by 3-D inverse modeling technique, has delivered useful constraints both to reconstruct the Vulcano Island evolution and to be used as input data for volcanic hazard assessment models. Our results constrained the depth and geometry of the main geo-structural features revealing more subsurface volcanic structures than exposed ones and allowing to elucidate the relationships between them. The recognition of two different magnetization sectors, approximatively coincident with the structural depressions of Piano caldera, in the southern half of the island, and La Fossa caldera at the north, suggests a complex structural and volcanic evolution. Magnetic highs identified across the southern half of the island reflect the main crystallized feeding systems, intrusions and buried vents, whose NNW-SSE preferential alignment highlights the role of the NNW-SSE Tindari-Letojanni regional system from the initial activity of the submarine edifice, to the more recent activity of the Vulcano complex. The low magnetization area, in the middle part of the island may results from hydrothermally altered rocks. Their presence not only in the central part of the volcano edifice but also in other peripheral areas, is a sign of a more diffuse historical hydrothermal activity than in present days. Moreover, the high magnetization heterogeneity within the upper flanks of La Fossa cone edifice is an imprint of a composite distribution of unaltered and altered rocks with different mechanical properties, which poses in this area an high risk level for failure processes especially during volcanic or hydrothermal crisis.

Keywords: Vulcano Island, magnetic survey, 3D inverse model, volcanic complex.

Introduction

The definition of the internal structure of an active volcano is of primary importance to fully understand the eruptive processes, to reveal its volcanic history, and to identify the main volcanic

Corresponding author, e-mail address: rosalba.napoli@ingv.it (R. Napoli)

37 and tectonic subsurface structures. Since regional and local structures, that are not often exposed,
38 may play an important role on volcanic evolution, they should be clearly detected and their link
39 with the eruptive processes should be elucidated.

40 Vulcano Island is an active volcanic complex which is potentially affected by significant
41 geohazards associated with the activity of the magmatic and hydrothermal systems. Indeed, even if,
42 in recent times no magmatic eruptions have taken place at the island, sudden and intense changes in
43 a set of geophysical and geochemical monitored parameters have been periodically observed. These
44 episodes have been characterized by simultaneous increase in the fumaroles temperatures and in the
45 gas emission rate, and by changes in the chemical composition toward more magmatic signatures,
46 which are generally accompanied by low magnitude seismic-volcanic sequences located below La
47 Fossa cone (Chiodini et al., 1992; Aubert et al., 2008; Alparone et al., 2010). These manifestations
48 reflect the strong activity of the hydrothermal system in La Fossa area and, even if no evidence of
49 magmatic rising has been recently observed (Granieri et al., 2006), it cannot be excluded that a
50 possible unrest can lead to violent phreatomagmatic eruptions, as happened in the past (Frazzetta
51 and La Volpe, 1991). Moreover, flank instability and failure with the subsequent formation of
52 tsunamis, can occur during period of unrest, as happened in 1988 (Tinti et al., 1998, De Astis et al.,
53 2003), since they can be triggered by dynamic phenomena, associated with the eruptive activity,
54 such as intrusions and earthquake swarms, and by the hydrothermal processes also in the absence of
55 the injection/intrusion of new magmatic fluids.

56 Although Vulcano had been extensively studied from volcanological, geochemical and geophysical
57 point of view (Chiarabba et al., 2004; Revil et al., 2008) and different models, from 2D to 2.75D
58 (Blanco-Montenegro et al., 2007), of its structural system have been produced, these models
59 represent a first-order approximation of the internal structure of the volcanic complex. This is due to
60 the several assumptions made throughout the modeling process, such as the infinite length of the
61 structures in strike direction in the 2D modeling techniques, the constant geometry and finite length
62 of buried bodies along the strike in 2.5D modeling, or the possible structural inconsistencies in the
63 geometrical arrangement of units from one cross-section to the other related to the need that the
64 section to be modeled is perpendicular to the structures direction. On the contrary, 3D modeling
65 techniques consider any shape of structures in any direction of space improving considerably
66 geologic interpretation. Up to date, no 3D modeling of Vulcano complex has been performed and
67 not all the relationships between subsurface structures and the surficial deposits have been clearly
68 elucidated, indeed some of them are still inferred or speculated (De Astis et al., 2013) exclusively
69 on the basis of the available geological and geophysical data. Recently, magnetic field imaging has
70 strongly contributed to a better understanding of the internal structure and evolution of different

volcanic systems such as maar volcanoes (Blaikie et al., 2014), volcanic seamount (Napoli et al., 2007), large calderas (Finn and Morgan, 2002) and composite volcano (Nicolosi et al., 2014). In this paper, ground and marine magnetic data gathered in 1989, 1994 (Del Negro et al., 1997) and 2001 over the entire island have been processed and a detailed magnetic anomaly map has been obtained. In order to recover 3D subsurface magnetization distribution responsible for the detected magnetic anomalies, we invert the magnetic data using a quadratic programming (QP) algorithm with bound constraints on remanent magnetization values. We obtain a 3D model, which, besides to being in agreement with geological and geophysical information already gathered over the island (Chiarabba et al., 2004; Blanco-Montenegro et al., 2007; De Astis et al., 2013), provides a better definition of the size and geometry of the buried volcanic bodies. Moreover, the modeling results elucidate the relationships between the main tectonic and volcanic features of the shallow part of the volcanic complex, up to 1 km below sea level (b.s.l.), which are not fully exposed since hidden by the growth of the overlying volcanic successions.

Geological setting and previous geophysical studies

Vulcano Island belongs to a NW-SE elongated submarine volcanic ridge that lies inside a graben-like structure (Iacobucci, 1977, Barberi et al., 1994) and rises more than 1 km from the continental slope (Romagnoli et al., 2013). The ridge develops along two main systems of NW–SE trending right-lateral strike-slip faults, parallel to the NW-SE Tindari-Letojanni system, which represents the northward propagation of the regional discontinuity of the Malta escarpment (Ventura et al. 1999) and extends up to NE Sicily (De Astis et al., 2003; De Ritis et al., 2005) intersecting the NE–SW and E–W features of the southeastern Tyrrhenian margin (Gabbianelli et al. 1991). Although Vulcano structural pattern is generally dominated by a NNW–SSE trend, representing a surficial expression of the Tindari–Letojanni system, minor N-S to NE-SW trending normal faults and cracks are also reported by Ventura et al. (1999) and associated to the main NW–SE shear zone. In particular, they described as tensional features and horsetails, strongly controlled the younger stages of the island development (De Astis et al., 2003, Iacobucci, 1977, Barberi et al., 1994). The subaerial morphology of the island is characterized by two main overlapping structural depressions more than 2.5 km wide, named the Piano caldera and La Fossa caldera, located on the southeastern and northwestern parts of the island, respectively (Fig.1). They are bounded by the NNW–SSE, N–S and NE–SW-trending lineaments (Mazzuoli et al., 1995; Ventura et al., 1999) and consequently interpreted as pull-apart-type basins with a negligible volcano tectonic or volcano-related component (De Astis et al., 2013). The pyroclastic edifice of Vulcanello and its lava platform form

106 a roughly circular peninsula on the northern tip of the island, while La Fossa cone, a 390 m high
107 composite edifice, is located within the central sector of La Fossa caldera (Chiarabba et al., 2004;
108 Revil et al., 2008).

109 The dated volcanism, occurred from about 130 ka to present times, has been characterized by a
110 wide spectrum of eruptive-explosive activities, including explosive phreatic and phreatomagmatic
111 eruptions producing wet and dry pyroclastic surges, pumice fall deposits, and highly viscous lava
112 flows (Frazzetta and la Volpe 1991; De Astis et al., 2013). Since the last eruption of La Fossa cone,
113 occurred from 1888 to 1890, the volcano activity has been characterized by recurrent thermal and
114 seismic crises due to magma-water interaction (Federico et al., 2010; Alparone et al., 2010). An
115 active hydrothermal system has been detected beneath La Fossa caldera, between 500 and 1,000 m
116 b.s.l. by gravity, seismological and geochemical studies (Berrino 2000; Chiodini et al., 1992;
117 Alparone et al., 2010). Intense fumarolic emissions are concentrated within La Fossa crater where a
118 few high temperature (400-500 °C) zones are active (De Astis et al., 2003), and on the southern and
119 northern flanks of the edifice, especially in the Grotta Palizzi area, and in the area of the Porto di
120 Levante harbor (Fig. 1), where also SP and CO₂ anomalies were identified and temperatures
121 generally do not exceed 98°C (Barde-Cabusson et al., 2009). Strong increases in fumaroles
122 temperature and in superficial manifestations, with a remarkable enlargement of the exhalative area
123 and a progressive increase in the gas emission rate, are generally observed when input of fluids of
124 magmatic origin occurs even without evidence of magmatic rising, as happened in 2004-2006. In
125 these cases the anomalous degassing episodes could derive from changes in rock permeability
126 (Todesco, 1997; Harris et al., 2012) or reflect a pulsating degassing process from a deep pressurized
127 stationary magma body (Granieri et al., 2006).

128 Since the first aeromagnetic and gravimetric surveys, dating back to the 70s, which characterized
129 the large-scale structures of Aeolian Islands including Vulcano (Iacobucci, 1977, Barberi et al.,
130 1994), several geophysical studies were executed at local scale to detect and define the shallow
131 structures of volcano complex. Valuable information on the subsurface structure of the La Fossa
132 caldera were obtained, by the intra-caldera sequences revealed by two deep geothermal drillings
133 (Fig.1) in 1983–1987 (Giocanda and Sbrana, 1991), located at the foot of the south-western and
134 northern flanks of the Fossa crater. The former encountered a shallow monzodioritic intrusion at
135 about 1350 m b.s.l., and reached a vertical depth of 2,050 m where a temperature of 419 C° was
136 founded. The second well, found a temperature of 243°C at 1,338 m and between 350 and 400°C at
137 1,578 m (Faraone et al. 1986). The entire pile revealed the occurrence of a differential collapse,
138 supporting a primary tectonic origin under control of the Tindari–Letojanni system for this caldera
139 (Gioncada & Sbrana, 1991).

140 Few gravity surveys were carried out on the Vulcano Island (Budetta et al., 1983; Sugihara et al.,
141 2002) and the data coverage is quite uneven, therefore, their interpretation is consequently limited
142 in areas scarcely covered. Anyway, two gravity highs were detected beneath the La Fossa crater and
143 inside the Piano caldera. The former was related to the self-sealed volcanics under which
144 geothermal fluids circulate, and the latter was ascribed to a rising discontinuity between superficial
145 loose pyroclastics and more compact underlying materials. A shallow seismic tomography (0-2 km
146 b.s.l.) obtained from the analysis of local earthquakes (Chiarabba et al., 2004) reconstructed the
147 geometry and distribution of main intrusions (intrusive bodies and lava pile), responsible for the
148 high-velocity anomalies, and recognized some intra-caldera depressions filled by pyroclastics, tuffs
149 and hyaloclastites, related to the low-velocity anomalies. Different high-resolution aeromagnetic
150 surveys were carried out in the last years (De Ritis et al., 2005; Blanco-Montenegro et al., 2007)
151 which revealed magnetic anomalies ascribable to the main crystallized feeding systems, intrusions,
152 and buried vents. In particular, Blanco–Montenegro et al. (2007) highlighted a large volume of
153 hydrothermally altered materials in La Fossa caldera area suggesting a larger hydrothermal system
154 than the active one. The results from aeromagnetic studies, in agreement with the tomography
155 support that the volcano complex has grown under the control of the Tindari-Letojanni fault system
156 and the associated N-S extensional faults (De Ritis et al., 2005), these last structures, in particular,
157 strongly controlled the uprising of magma and the location of eruptive vents at depth lesser than 0.5
158 km b.s.l. This is also confirmed by the few available bathymetric and seismic data (Gabbianelli et
159 al., 1991; Favalli et al., 2005; Romagnoli et al., 2013), which revealed on the western flank of the
160 volcano complex some submarine volcanic features aligned along NNW–SSE regional trends,
161 related to the early stage of its development. While, volcanic features ascribable to a more recent
162 activity appear radially elongated along the submarine southern and eastern flanks.

163

164 ***Magnetic data***

165

166 The survey strategy is aimed to capture the Vulcano Island magnetic signatures and to correlate
167 them with the main volcanic and tectonic features in order to image the subsurface structures of the
168 volcanic complex in a 3D framework. More than 18,000 magnetic data were retrieved from three
169 high resolution ground magnetic surveys carried out at Vulcano Island in 1989, 1994 and 2001.
170 Shipborne data were also gathered offshore in 1994, along a profile parallel to the coast line, to
171 constrain the magnetic field just a few tens meters from the coast. Practically, the surveys cover the
172 emerged tip of the volcanic edifice, for about 42 km², corresponding to the entire island. Data were
173 acquired along lines describing an irregular grid (Fig. 1A) by an ELSEC 770, a Geometrics G-856
174 and an Overhauser effect magnetometer. During each survey a base station was used to correct for

175 the magnetic external variations (Del Negro et al., 1997). The magnetic surveys were carried out
176 during days characterized by geomagnetic K index values < 2 , ensuring a suitable data accuracy in
177 the removal of time variations of external origin. Moreover, International Geomagnetic Reference
178 Field (IGRF) models available at the time of the three different surveys (IGRF-4, IGRF-5 and
179 IGRF-8) have been subtracted to make the data comparable. Finally, the data from these three
180 surveys were merged to provide a data set for the entire area. Therefore, in order to obtain the
181 magnetic anomaly map, data were reduced to a regular grid with a constant spacing of 0.5 km using
182 a minimum curvature algorithm, ending up with a final dataset of 4521 observational points. A
183 regional field was then estimated that linearly fitted the magnetic data by the least-squares criterion,
184 and was subsequently subtracted from them. The total-intensity residual anomaly map is shown in
185 Fig. 1B. To suppress spurious anomalies related to shallow magnetic sources, data were upward
186 continued (Fig. 2A) to a constant altitude of 550 m, namely 50 m from the highest elevation of the
187 island (Mt. Aria). The data highlight intense maximum in the La Fossa cone south-eastern flank.
188 Other magnetic highs, NNW-SSE elongated, dominate the Piano caldera rims. In particular, along
189 the western rim of Piano caldera a maximum with a sub-elliptical shape extends for about 3 km
190 parallel to the caldera rim overlapping, from south to north, the Timpe del Corvo, the Scoglio
191 Conigliara and the Mt. Saraceno basaltic cone. Also the eastern rim of the caldera is characterized
192 by the presence of a high magnetization area, elongated in the NNW-SSE direction for about 1 km,
193 but in this case no surface evidence of eruptive centers is observed. Another maximum with a
194 regular circular shape appears well isolated in the central area of the caldera. On the contrary, a
195 wide area of low magnetization spreads in the middle part of the island, within La Fossa caldera in
196 the sea sector between Vulcanello and La Fossa cone and in the area of Grotta Palizzi. The main
197 magnetic anomalies detected are in agreement with those obtained by the previous aeromagnetic
198 surveys (De Ritis et al., 2005; Blanco-Montenegro et al., 2007), even if the very close sampling step
199 of 3 m adopted during our ground magnetic surveys allowed to highlight shorter wavelengths
200 related to very shallow magnetic features. In particular, in the resulting magnetic anomaly map the
201 shape of the magnetic anomalies appear more articulated and their locations are better defined than
202 previous studies.

203

204

205 ***Imaging of Vulcano Island***

206 A 3-D subsurface magnetization model was obtained by a Quadratic Programming algorithm
207 (Napoli et al., 2007). In order to allow the maximum flexibility for the model to represent
208 geologically realistic structures, the island was represented as a crustal block of $8.5 \times 6.7 \text{ km}^2$ in area

209 and 1.5 km in thickness. Indeed, the crustal block extends offshore to take into account the side
210 effect of the source bodies surrounding the observational area. The ground surface was generated
211 from a digital elevation model of Vulcano Island from the 30 m Shuttle Radar Topography Mission
212 (SRTM) data and the GEBCO bathymetry database (<http://www.gebco.net>). The crustal block was
213 discretized into a set of rectangular prisms. Horizontal and vertical dimensions of rectangular
214 prisms were taken as variables (Fig. 3) to account for the higher resolution required in diverse areas.
215 In particular, in order to better approximate the topographic relief, we considered a set of prisms
216 above the sea level, each $0.125 \times 0.125 \times 0.125 \text{ km}^3$ in size. Below sea level, prisms have 0.25×0.25
217 km^2 horizontal area and a thickness of 0.25 km. Finally, the bottom depth of the model was
218 assumed to be 1.0 km b.s.l., thus formalizing an inversion problem with 8921 unknowns on the
219 magnetization values. The depth resolution is closely related to the extension of the survey (Fedi
220 and Rapolla, 1999). The anomaly field was inverted assuming that the average direction of the total
221 magnetization is close to Earth's present-day field direction (inclination of 54°N , declination of
222 0.9°W). The remanent magnetization is generally much greater than induced magnetization and
223 rocks of Vulcano Island were emplaced about 135 ka (De Astis et al., 2003) after the last field
224 reversal (786 ka, Lowrie and Kent 2004). Parameters used for the data inversion are summarized in
225 Table 1.

226 Volcanic rocks are usually highly magnetic due to their relatively high magnetite content. The
227 intensity of magnetization of these rocks is largely dependent upon several factors such as the
228 magma composition, cooling rate, grain size, volatile content and alteration history. Therefore, the
229 intensity of magnetization is extremely variable and there can be considerable overlap between
230 different lithologies (Kearey and Brooks, 1991). Anyway, high values (up to 10 Am^{-1}) of intensity
231 of magnetization are generally generated by high concentrations of magnetite and small grains that
232 usually are associated to magma intrusions and compact lava flows, on the contrary low values (few
233 Am^{-1}) are related to low concentrations of magnetite and to the presence of larger grains such as it
234 has been observed in volcanoclastic deposits (Hildebrand, Rosenbaum & Kauahikaua, 1993; Napoli
235 et al., 2007).

236 In Vulcano Island the great variety of erupted volcanic products (lava flows, dikes, pyroclastic
237 deposit, etc..) produces a significant heterogeneity in rock magnetic properties. In particular,
238 laboratory tests executed on rock specimens (Zanella and Lanza, 1994) of Vulcano Island revealed
239 that the highest magnetization values correspond to the lavas of Vulcanello, followed by the lava
240 flow of Punta Roja, and the less magnetic lava flows are those of the Lentia edifice and the Fossa
241 cone, whereas lavas of the Primordial Vulcano show intermediate magnetization values. Ash
242 deposits of the Fossa caldera show the lowest total magnetization values in the island (Blanco-

243 Montenegro et al., 2007). In agreement with these results in the inversion procedure, we imposed
244 constraints on the intensity of natural remanent magnetization (JNRM) range from 0 to 10 Am⁻¹.
245 The accuracy on the obtained magnetization values was estimated from the square-root of the
246 diagonal elements of the inverse Q matrix (Gill et al., 1981). The accuracy is related to the prisms'
247 depth, location, and, in particular, it reaches a maximum value of about 0.9 Am⁻¹ for deeper prisms,
248 whereas it is below 0.6 Am⁻¹ for shallower ones.

249 The computed field well matches with the observed one with residuals having a standard deviation
250 of 8 nT (Figs. 2B, C). The volcano magnetization model resulting from the constrained inversion of
251 data set is shown in Fig. 4.

252 Horizontal layers from 250 m above sea level to 750 m below sea level (Fig.4), and N-S and E-W
253 sections (Fig. 5) provide a detailed imaging of the shallow part of the volcanic complex. The
254 southern part of the island is characterized by a NNW-SSE alignment of different magnetization
255 highs, with an intensity greater than 8 Am⁻¹, located along the Piano caldera rims. The magnetic
256 structures observed along the western rim can be related to the presence of magnetic bodies
257 associated to feeding conduits of eruptions and magmatic intrusions that supplied the construction
258 of Mt. Saraceno basaltic cone (8 ka, De Astis et al., 2003), and to non-outcropping mafic massive
259 rocks along the Timpa del Corvo eruptive fissure, extending further south, parallel to the caldera
260 rim.

261 Both the intensity and areal extent increase with depth reaching the maximum value of 9 Am⁻¹ and
262 over 3 km in length respectively, at the sea level where the magmatic feeding systems seem to be
263 connected each other forming a single volume (Fig. 6) along the NNW–SSE trend that is one of the
264 main regional fault systems (the Tindari-Letojanni system) characterizing Vulcano Island (De Astis
265 et al., 2013). It is reasonable to suppose that this assumed preferential pathway for magma ascent,
266 strongly controlled by the regional stress field, and by the minor associated N–S to NE–SW trending
267 extensional structures has also produced the basaltic lava flows outcropping near Scoglio Conigliara
268 in the central part of this Piano caldera rim. Indeed, the proximity between this important magnetic
269 structure and these lava flows strongly suggests a clear correlation between them. Moreover, till
270 now, no surface evidence of the eruptive vents from which these lava flows were outpoured has
271 been detected, and due to the limited exposures, a certain identification of the source area was not
272 possible (De Astis et al., 2013).

273 Below the sea level (Fig.4) the magnetic high related to the Timpa del Corvo fissure becomes
274 smaller and disappears at 0.75 km b.s.l. On the contrary, beneath Mt Saraceno cone, at the junction
275 between the Piano caldera and La Fossa caldera structures, the magnetized volume is still present
276 with a magnetization of about 5 Am⁻¹, showing the presence of magnetized rocks reasonably related

277 to a previous activity in this area. This region was already identified by Blanco-Montenegro et al.
278 (2007) from aeromagnetic data and was supposed to be the remnants of an early submarine volcano.
279 Other two different magnetization highs were observed along the eastern rim of the caldera. The
280 former is centered beneath Mt. Luccia at the northeast edge of the caldera rim, while the latter
281 marks the eastern rim of the caldera where no volcanic center outcrops. Both of them are
282 characterized by a magnetization intensity of about 8 Am^{-1} , that is a high value generally associated
283 to massive intrusions and/or feeding systems of volcanic centers, and show a NNW-SSE
284 preferential alignment. These evidences suggest that also in this area of the island the Tindari-
285 Letojanni regional fault system and the associated N–S to NE-SW striking normal faults could have
286 produced favorable conditions for magma ascent. This area is characterized by the presence of the
287 Piano di Luccia formation, welded strombolian to hawaiian fallout products filling the Piano
288 caldera, whose source area has been speculated (De Astis et al., 2013) but has not yet been clearly
289 identified. Considering the proximity between the Piano Luccia formation and the detected
290 magnetic highs, it is reasonable to assume that they are related to each other and suppose that the
291 outcropping products are the results of the activity originated from these volcanic features. In the
292 middle of Piano caldera the 3D model reveals at very shallow depths a wide area of low
293 magnetization intensity of about 2 Am^{-1} ascribed to pyroclastic products. Magnetization highs
294 appear with increasing depth. Indeed, two magnetized volumes with an intensity of about 8 Am^{-1}
295 are detected at the north of Mt. Aria and may be related to the presence of magnetic bodies
296 interpreted as the feeding conduits of basaltic eruptions and magma intrusions that supplied the
297 construction of the Monte Rosso volcanic center.

298 Within La Fossa caldera a very low magnetization area is observed in correspondence of the
299 northern and western flanks of La Fossa cone. This magnetic signature could be related to the low
300 magnetization of pyroclastic deposits forming this part of the volcanic edifice (Blanco et al., 2007),
301 that, however, do not cover all the inferred low magnetized volume. Two other possible hypotheses
302 can be proposed to properly account for the origin of this low magnetization volume. As a first
303 hypothesis, the low magnetization could be ascribed to thermal demagnetization processes
304 generated by heat transfer from the subcrustal magma chamber. Regarding this hypothesis, at
305 Vulcano the Curie temperature of most lithotypes, ranges between 550 and 580°C (Zanella and
306 Lanza 1994), that is reached at 1.5-3 km depth (De Ritis et al., 2013) and pyroclastic products lose
307 50% of their initial magnetization already at 200°C (Zanella and Lanza 1994). These high
308 temperatures are encountered by drillings only at depths greater than 1 km (Faraone et al., 1986),
309 that is below the bottom of our model. This excludes the hypothesis of thermal demagnetization
310 processes generated by volcano-scale heating in the investigated volume. As a second hypothesis,

311 the presence of intense fumarolic emissions whose temperature, during episodes of unrest, can
312 increase up to 700°C in very limited spaces (fumarolic conduits and vents), (De Astis et al., 2003;
313 Granieri et al., 2006) and the evidence of limited thermoelastic deformation enhanced in this zone
314 (Bonaccorso et al., 2010), favor a more straightforward explanation in terms of hydrothermal
315 alteration which can decrease, and even nullify the magnetic signature of the volcanic host rocks
316 (Reid et al., 2001; Tivey and Dymment, 2010).

317 Although, the whole La Fossa cone is covered by pyroclastic deposits, the 3 D model reveals in the
318 eastern flank of the volcanic edifice a magnetized body with intensity of about 8Am^{-1} elongated in
319 the North-South direction for about 1 km. It corresponds to the high-velocity body found by
320 Chiarabba et al. (2004), and can be related to the lava flows that were emitted during the early
321 volcanic activities of La Fossa cone (Keller, 1980) and that outcrop at its northeastern base (De
322 Astis et al., 2013). With increasing depth, magnetization and areal extension diminish, but at about
323 0.5 km b.s.l. the magnetized volume is still present. For this magnetic body we obtained a
324 horseshoe-shaped volume of about $5.3 \times 10^7 \text{ m}^3$ (Fig. 6), and considering the high magnetization
325 values we can interpret it as the magmatic feeding system of this eruptive center suggesting a more
326 significant effusive activity than that speculated on the basis of lava flows outcropping.

327 Another low magnetization area, with intensity less than 1 Am^{-1} , is observed in the western sector
328 of La Fossa caldera, where it overlays a part of the active hydrothermal system, in the sea sector
329 between Vulcanello and La Fossa cone and in the area of Grotta Palizzi, and a part of the well-
330 known depression between the Lentia domes and La Fossa cone (Fig. 4). This area, which is filled
331 by tuffs, pyroclastics and hyaloclastites (Giocanda and Sbrana, 1991), is characterized by low
332 magnetization values, $0\text{-}2 \text{ Am}^{-1}$, (Giocanda and Sbrana, 1991; Blanco-Montenegro et al., 2007) and
333 is coincident with the low Vp zone detected by the seismic tomography of the island (Chiarabba et
334 al. 2004).

335 Northwest, in correspondence with the Lentia complex, the model reveals an area of magnetization
336 intensity of about 4 Am^{-1} with a N-S orientation. This value is comparable to that associated to the
337 subaerial lava flows and domes of the Lentia complex (Blanco-Montenegro et al., 2007). At
338 Vulcanello, small magnetized volumes with intensity of 8 Am^{-1} are detected and are well correlated
339 with the high seismic velocity (Vp) zone (Chiarabba et al., 2004) and associated to leucite-bearing
340 lava platform forming Vulcanello (Fig.4). The magnetization intensities observed both at Lentia and
341 at Vulcanello diminish with increasing depth and the relative sources seem to be confined to the
342 shallow part of the volcano supporting the idea that they are related to the most recent phases of the
343 volcano activity. From 250 to 750 m b.s.l. the magnetization intensity drastically diminishes over
344 the whole island and its distribution appears more homogeneous. Magnetized highs are founded in

the northwest and northeastern areas of the island, but not completely described since they continue offshore where no measurements were gathered. Anyway, they seem to be in good agreement with the offshore anomalies detected and interpreted by De Ritis et al., (2005), as the crystallized Lentia plumbing system and Vulcanello lavas. Below 0.5 km b.s.l., only the NNW-SSE oriented magnetic volume persists inside the Piano caldera, where it has been speculated the presence of the main feeding system which gave rise to the Primordial Vulcano (Keller, 1980; De Astis et al., 1997; 2013). Other two magnetic structures are still present in correspondence of La Fossa cone and Mt Saraceno representing the deeper and consequently the older volcanic structures here recognizable on the basis of the data resolution.

354
355

356 **Discussions and conclusion**

Following the 3D magnetization model the volcanic complex of Vulcano Island can be divided in two different sectors approximatively coincident with the structural depressions of Piano caldera, in the southern half of the island, and La Fossa caldera at the north. The former, is characterized by clusters of high-magnetization (about 9 Am^{-1}) regions, the most intense over the island, detected along the rims and within the Piano caldera, which correspond to the main eruptive centers of this sector of the island, such as Timpe del Corvo, Scoglio Conigliara, Mt. Rosso and Punta Luccia, and represent the magnetic signatures of their feeding systems, massive intrusions, and buried vents. Their extension reveals more subsurface magmatic volumes and/or shallow and local volcanic structures than exposed ones. The 3D model provides a detailed definition of the size and geometry of these subsurface structures (Fig. 5) allowing to elucidate the relationships between them and to link them to surface deposits such as lava flows of Scoglio Conigliara and Piano Luccia formation, whose source areas were not previously detected. These volcanic features appear structurally controlled by the NNW-SSE regional structural lineament at any depth, supporting the key role played by the Tindari-Letojanni system in controlling the location and shape of the volcanic edifices from the initial activity of the submarine edifice, to the more recent activity of Mt Saraceno. On the other hand, in the more recent La Fossa caldera sector the NNW-SSE preferential alignment is not so evident. In particular, in this area only a few magnetized highs were detected: (i) a N-S magnetic body along the eastern flank of La Fossa cone (ii) the Lentia complex N-S magnetized volume along the western rim of the caldera, and (iii) the intensely magnetized volumes of Vulcanello. The Lentia complex and Vulcanello lavas are detected only in the shallow part of the model, up to 250 m b.s.l., and none of them shows the NNW-SSE alignment. This largely follows the suggestions of Mazzuoli et al. (1995) and Ventura et al. (1999) that the most recent phases of the volcano activity

379 were controlled by north–south to NE–SW tectonic lineaments and the Tindari-Letojanni system no
380 longer dominated.

381 In La Fossa caldera sector, large zones of reduced magnetization are mainly concentrated in the
382 shallowest layers. They are the evidence for alteration related to hydrothermal processes and extend
383 over a region wider than that affected by the current active hydrothermal system. This suggests that
384 in the past the hydrothermal system had a greater extension and had primarily developed in this area
385 of the island. On the basis of available data, it is not possible to assert if there was a really large
386 active area at some time, or alternatively different areas were active at different times. Both
387 conditions may have occurred or more probably they may have coexisted.

388 Finally, our results reveals low magnetized volumes forming the northern and southern flanks of La
389 Fossa cone edifice, that could be reasonably ascribed to pyroclastic and hydrothermally altered
390 rocks. These flanks are bounded eastwards by a significant volume of lava pile which may be less
391 permeable and consequently less amenable to hydrothermal alteration than the other parts of La
392 Fossa cone acting as an impermeable limit to the fluids circulation. This could explain the fumarolic
393 emission patterns, which are not spread homogenously in the La Fossa area but are locally
394 concentrated in the northern and southern flanks formed by more permeable pyroclastic deposits.
395 Their relatively steep slopes, the active fluids circulation, proved by the presence of fumaroles and
396 hydrothermal alteration, could promote large collapses in these areas, which can more easily
397 undergo flank failure. Therefore, in case of volcanic or hydrothermal crisis a high level of hazard is
398 posed to these flanks of the volcano, especially in the transition zones between the hydrothermally
399 altered rocks and lava pile.

400 By providing a detailed description of the main geo-structural features and of distributions of
401 unaltered and altered rocks, our findings from the 3D magnetic imaging provide new constraints to
402 be used in aiding the Vulcano Island hazard assessments.

403

404 **Acknowledgements**

405 We are indebted to the researchers and technicians of the INGV-Osservatorio Etneo for performing
406 magnetic surveys. We are grateful to Tony Hurst, Jean-Francoise Lenat and the Editor Jurgen W.
407 Neuberg for their helpful comments which improve the manuscript.

408

409

410

411

412

References

- Alparone, S., Cannata, A., Gambino, S., Gresta, S., Milluzzo, V., Montalto, P., 2010. Time-space variation of the volcanoseismic events at La Fossa (Vulcano, Aeolian Islands, Italy): new insights into seismic sources in a hydrothermal system. *Bull. Volcanol.* 72, 803–816.
- Aubert, M., Diliberto, S., Finizola, A., Chébli, Y., 2008. Double origin of hydrothermal convective flux variations in the Fossa of Vulcano (Italy). *Bull. Volcanol.* 70:743–751, DOI 10.1007/s00445-007-0165-y.
- Barberi, F., Gandino, A., Gioncada, A., La Torre, P., Sbrana, A., Zenucchini, C., 1994. The deep structure of the Eolian arc (Filicudi–Panarea–Vulcano sector) in light of gravity, magnetic and volcanological data. *J. Volcanol. Geotherm. Res.* 61:189–206.
- Barde-Cabusson, S., Finizola, A., Revil, A., Ricci, T., Piscitelli, S., Rizzo, E., Angeletti B., Balasco, M., Bennati, L., Byrdina S., Carzaniga, N., Crespy, A., Di Gangi, F., Morin, J., Perrone, A., Rossi, M., Roulleau, E., Suski, B., Villeneuve, N., 2009. New geological insights and structural control on fluid circulation in La Fossa cone (Vulcano, Aeolian Islands, Italy). *J. Volcanol. Geotherm. Res.* 185, 231–245.
- Berrino, G., 2000. Combined gravimetry in the observation of volcanic processes in Italy. *J. Geodyn.* 30:371–388.
- Blaikie, T. N., Ailleres, L., Betts, P.G., Cas, R. A. F., 2014. Interpreting subsurface volcanic structures using geologically constrained 3-D gravity inversions: Examples of maar-diatremes, Newer Volcanics Province, southeastern Australia. *J. Geophys. Res. Solid Earth*, 119, 3857–3878, doi:10.1002/2013JB010751.
- Blanco-Montenegro, I., de Ritis, R., Chiappini, M., 2007. Imaging and modelling the subsurface structure of volcanic calderas with high-resolution aeromagnetic data at Vulcano (Aeolian Islands, Italy). *Bull. Volc.*, 69, 643–659, doi:10.1007/s00445-006-0100-7.
- Bonaccorso, A., Bonforte, A., Gambino, S., 2010. Thermal expansion-contraction and slope instability of a fumarole field inferred from geodetic measurements at Vulcano. *Bull. Volcanol.* DOI 10.1007/s00445-010-0366-7.
- Budetta, G., Nunziata, C., Rapolla, A., 1983. A gravity study of the island of Vulcano, Tyrrhenian Sea, Italy. *Bull. Volcanol.* 46:183–192.
- Chiarabba, C., Pino, N.A., Ventura, G., Vilaro, G., 2004. Structural features of the shallow plumbing system of Vulcano Island Italy. *Bull. Volcanol.* 66, 477–484.
- Chiodini, G., Cioni, R., Falsaperla, S., Guidi, M., Marini, L., Montalto, A., 1992. Geochemical and seismological investigations at Vulcano (Aeolian islands) during 1978–1989. *J. Geophys. Res.* 97:11025–11032.

- 447 De Astis, G., Ventura, G., Vilardo, G., 2003. Geodynamic significance of the Aeolian volcanism
448 (southern Tyrrhenian Sea, Italy) in light of structural, seismological and geochemical data.
449 *Tectonics*, 22, 4 DOI 10.1029/2003TC001506.
- 450 De Astis, G., Lucchi, F., Dellino, P., La Volpe, L., Tranne, C. A., Frezzotti, M. L., Peccerillo, A.,
451 2013. Geology, volcanic history and petrology of Vulcano (central Aeolian archipelago).
452 *Geological Society, London, Memoirs* 2013, 37; p281-349. doi: 10.1144/M37.11.
- 453 De Ritis, R., Blanco-Montenegro, I., Ventura, G., Chiappini, M., 2005. Aeromagnetic data provide
454 new insights on the tectonics and volcanism of Vulcano island and offshore areas (southern
455 Tyrrhenian Sea, Italy). *Geophys. Res. Lett.*, 32 (L15305). DOI 10.1029/2005GL023465.
- 456 Del Negro, C., Branciforte, M., Ferrucci, F., Napoli, R., Sicali, A., Tabacco, S., 1997. High
457 resolution magnetic survey of the Island of Vulcano. CCE funded TekVolc project, contract n.
458 EV5V-CT92-0191, report.
- 459 Faraone, D., Silvano, A., Verdiani, G., 1986. The monzogabbroic intrusion in the island of Vulcano,
460 Aeolian archipelago, Italy. *Bull. Volcanol.* 48:299–307.
- 461 Favalli, M., Karatson, R., Mazzuoli, R., Pareschi, M.T., Ventura, G., 2005. Volcanic
462 geomorphology and tectonics of the Aeolian archipelago (southern Italy) based on integrated
463 DEM data. *Bull. Volcanol.* 68:157–170. Federico, C., Capasso, G., Paonita, A., Favara, R., 2010.
464 Effects of steam-heating processes on a stratified volcanic aquifer: Stable isotopes and dissolved
465 gases in thermal waters of Vulcano Island (Aeolian archipelago). *J. Volcanol. Geotherm. Res.*
466 192, 178–190 doi:10.1016/j.jvolgeores.2010.02.020.
- 467 Fedi, M., Rapolla, A., 1999. 3-D inversion of gravity and magnetic data with depth resolution.
468 *Geophysics*, 64, 452–460.
- 469 Finn, C. A., Morgan, L.A., 2002. High-resolution aeromagnetic mapping of volcanic terrain,
470 Yellowstone National Park, *J. Volcanol. Geotherm. Res.*, 115(1–2), 207–231.
- 471 Frazzetta, G., La Volpe, L., 1991. Volcanic history and maximum expected eruption at “La Fossa
472 di Vulcano” (Aeolian Islands, Italy), *Acta Volcanol.*, 1, 107– 113.
- 473 Gabbianelli, G., Romagnoli, C., Rossi, P. L., Calanchi, N., Lucchini, F., 1991. Submarine
474 morphology and tectonics of Vulcano (Aeolian Islands, Southeastern Tyrrhenian Sea). *Acta*
475 *Vulcanologica*, 1, 135–142.
- 476 Gill, P.E., Murray, W., Wright, M.H., 1991. *Practical optimization*. Academic Press, London.
- 477 Gioncada, A. Sbrana, A., 1991. “La Fossa caldera”, Vulcano: inferences from deep drillings. *Acta*
478 *Vulcanol.*, 1, 115–125.
- 479 Granieri, D., Carapezza, M.L. Chiodini, G., 2006. Correlated increase in CO₂ fumarolic content and
480 diffuse emission from La Fossa crater (Vulcano, Italy): Evidence of volcanic unrest or increasing

481 gas release from a stationary deep magma body? *Geophys. Res. Lett.*, 33, L13316, doi:
482 10.1029/2006GL026460.

483 Harris, A., Alparone, S., Bonforte, A., Dehn, J., Gambino, S., Lodato, L., Spampinato, L., 2012.
484 Vent temperature trends at the Vulcano Fossa fumarole field: the role of permeability. *Bull.*
485 *Volcanol.* 74:1293–1311 DOI 10.1007/s00445-012-0593-1.

486 Hildenbrand, T.G., Rosenbaum, J.G., Kauahikaua, J.P., 1993. Aeromagnetic study of the Island of
487 Hawaii, *J. Geophys. Res.*, 98, 4099–4119.

488 Iacobucci, F., Incoronato, A., Rapolla, A., Scarascia, S., 1977. Basement structural trends in the
489 volcanic islands of Vulcano, Lipari, and Salina (Aeolian Islands, Southern Tyrrhenian Sea)
490 computed by aeromagnetic and gravimetric data. *Boll. Geofis. Teor. Appl.* 20:73–74, 49–61.

491 Kearey, P., Brooks, M., 1991. An introduction to geophysical exploration. Oxford, Blackwell
492 Scientific Publications, Second edition, pp. 1–254.

493 Keller, J., 1980. The island of Vulcano. *Rend. Soc. Ital. Mineral. Petrol.*, 36, 369–414. Lowrie, W.,
494 Kent, D.V., 2004. Geomagnetic polarity timescales and reversal frequency regimes. In: Channell
495 J.E.T., Kent D.V., Lowrie W., Meert J., editors. *Timescales of the Palaeomagnetic Field.*
496 *American Geophysical Union.* p. 117–129.

497 Mazzuoli, R., Tortorici, L., Ventura, G., 1995. Oblique rifting in Salina, Lipari and Vulcano Islands
498 (Aeolian Islands, Southern Tyrrhenian Sea, Italy). *Terra Nova*, 7, 444–452.

499 Napoli, R., Currenti, G., Del Negro, C., 2007. Internal structure of Ustica volcanic complex (Italy)
500 based on a 3D inversion of magnetic data. *Bull. Volcanol.* DOI 10.1007/s00445-007-0115-8.

501 Nicolosi, I., D'Ajello Caracciolo, F., Branca, S., Ventura, G., Chiappini, M., 2014. Volcanic conduit
502 migration over a basement landslide at Mount Etna (Italy). *Scientific Reports*, 4 : 5293. DOI:
503 10.1038/srep05293.

504 Reid, M.E., Sisson, T.W., Brien, D.L., 2001. Volcano collapse promoted by hydrothermal alteration
505 and edifice shape, Mount Rainier, Washington. *Geology*, 29, 9: 779–782.

506 Revil, A., Finizola, A., Piscitelli, S., Rizzo, E., Ricci, T., Crespy, A., Angeletti, B., Balasco, M.,
507 Barde Cabusson, S., Bennati, L., Bole' ve, A., Byrdina, S., Carzaniga, N., Di Gangi, F., Morin, J.,
508 Perrone, A., Rossi, M., Roulleau, E., Suski, B., 2008. Inner structure of La Fossa di Vulcano
509 (Vulcano Island, southern Tyrrhenian Sea, Italy) revealed by high-resolution electric resistivity
510 tomography coupled with self-potential, temperature, and CO₂ diffuse degassing measurements.
511 *J. Geophys. Res.*, 113, B07207–1, 21 doi: 10.1029/2007JB005394.

512 Romagnoli C., Casalbore, D., Bosman, A., Braga, R., Chiocci, F.L., 2013. Submarine structure of
513 Vulcano volcano (Aeolian Islands) revealed by high-resolution bathymetry and seismo-acoustic
514 data. *Marine Geology*, 338, 30–45, DOI: 10.1016/j.margeo.2012.12.002.

515 Sugihara, M., Okuma, S., Nakano, S., Furukawa, R., Komazawa, M., Supper, R., 2002.
516 Relationship between geothermal activity and gravity anomalies on Vulcano Island, Italy.
517 Proceedings 24th NZ Geothermal Workshop 2002.

518 Tinti, S., Bortolucci, E., Armigliato, A., 1998. Numerical simulation of the landslide-induced
519 tsunami of 1988 on Vulcano Island, Italy. Bull Volcanol 61 :121–137.

520 Tivey, M.A., Dymment, J., 2010. The magnetic signature of hydrothermal systems in slow spreading
521 environments, in Rona, P.A., Devey, C.W, Dymment, J., and Murton, B.J., eds., Diversity of
522 hydrothermal systems on slow spreading ridge: American Geophysical Union, Geophysical
523 Monograph Series, 188, 43–66.

524 Todesco, M., 1997. Origin of fumarolic fluids at Vulcano (Italy). Insights from isotope data and
525 numerical modeling of hydrothermal circulation. J. Volcanol. Geotherm. Res. 79, 63–85
526 doi:10.1016/S0377-0273(97)00019-X.

527 Ventura, G., Vilardo, G., Milano, G., Pino, N. A., 1999. Relationships among crustal structure,
528 volcanism and strike-slip tectonics in the Lipari-Vulcano volcanic complex (Aeolian Islands,
529 Southern Tyrrhenian Sea, Italy). Physics of the Earth and Planetary Interiors, 116, 31–52.

530 Zanella, E., Lanza, R., 1994. Remanent and induced magnetization in the volcanites of Lipari and
531 Vulcano (Aeolian Islands). Ann. Geophys. 37:1149–1156.

532

533

534

535

536

537

538

539

540

541

542

543

544

545

546

547

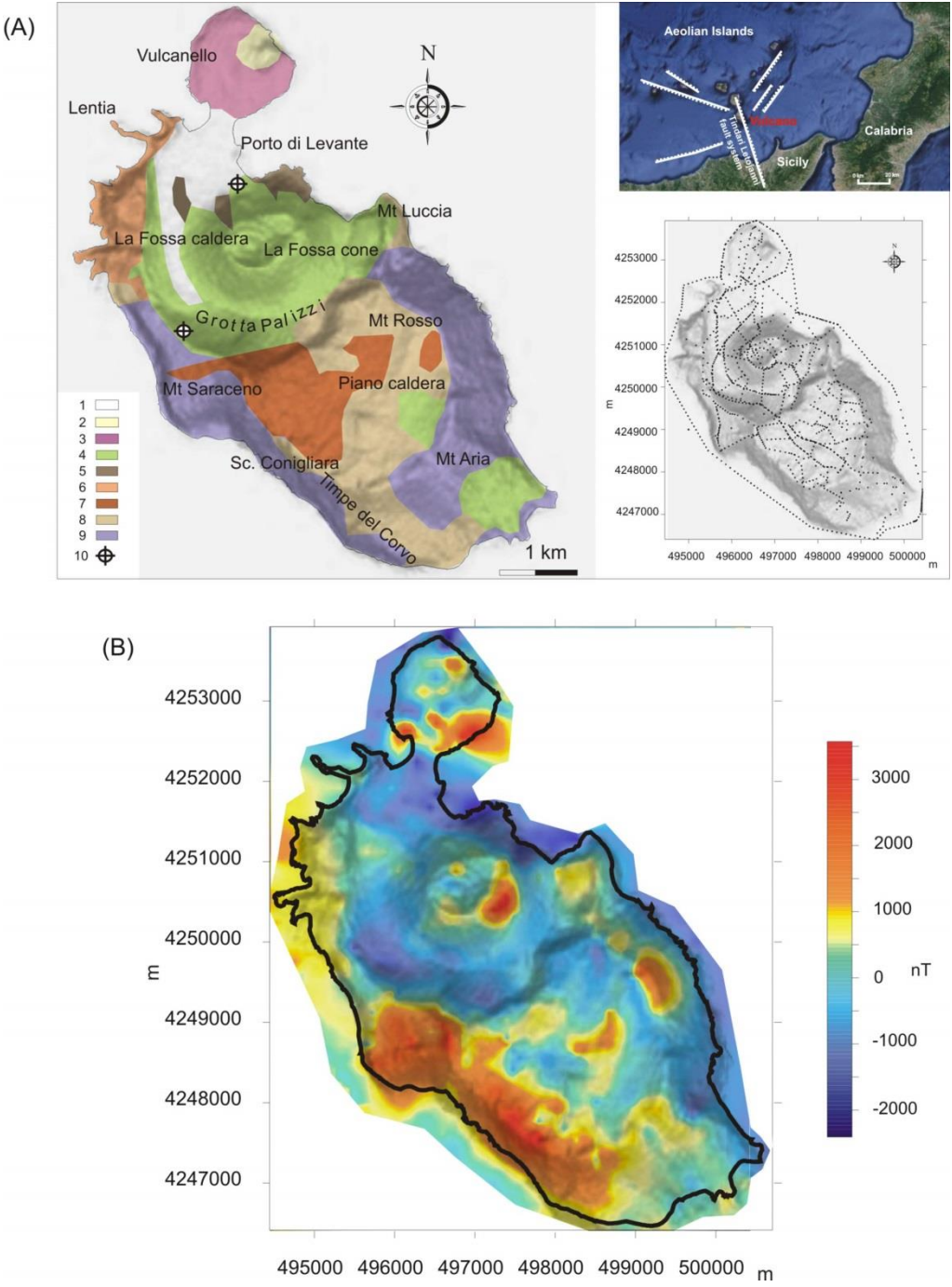
548

549

550

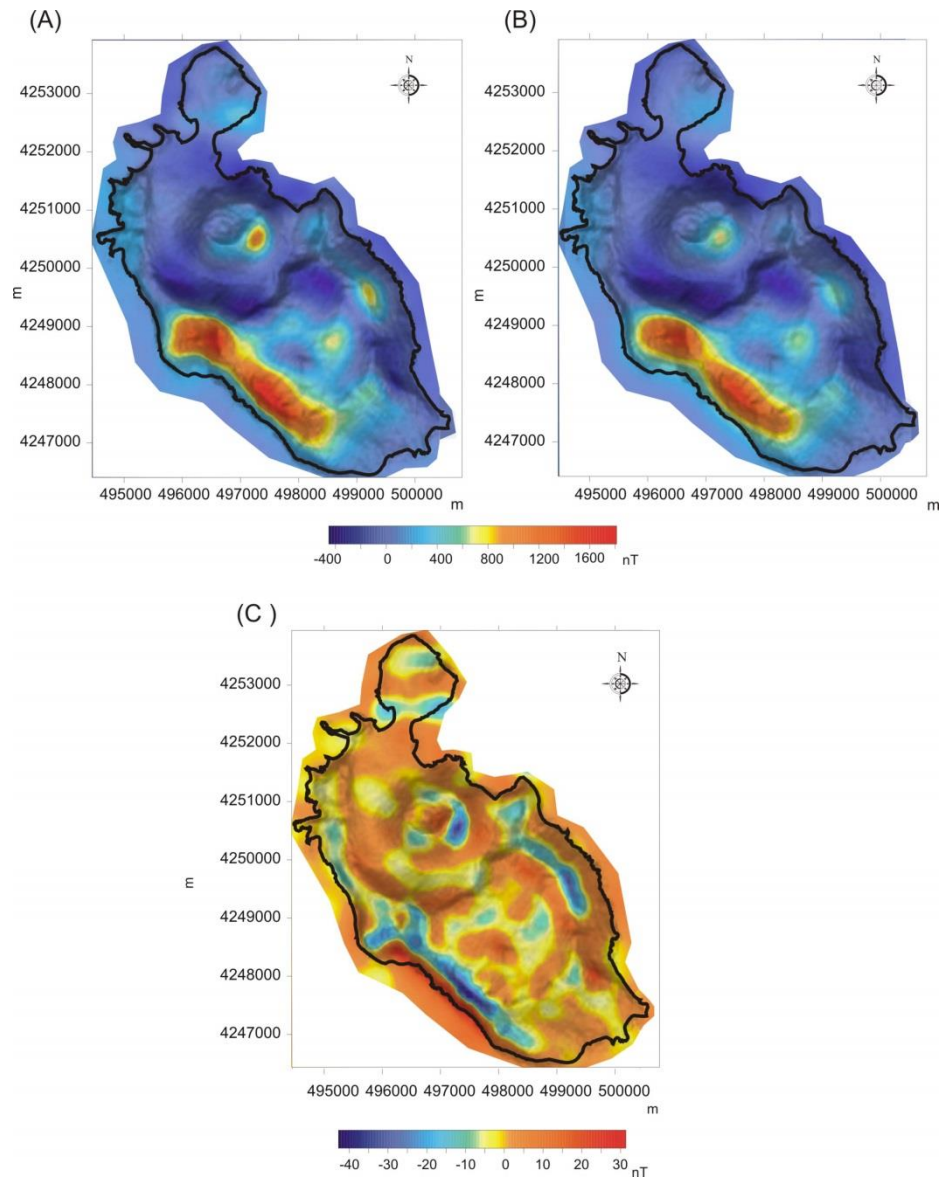
551

552 **Figure**
553



554
555

556 Figure 1 - (A) Simplified geological map of Vulcano Island. Legend: 1) alluvium and beach
557 deposits; 2) Vulcanello pyroclastics; 3) Vulcanello lava flows; 4) Fossa cone pyroclastics; 5) Fossa
558 cone lava flows; 6) Lentia domes and lava flows; 7) hyaloclastites and pillow lava; 8) lava flows
559 and minor pyroclastics; 9) South Vulcano lavas and scorias; 10) drilling location. In the inset the
560 black dashed lines represent measurement tracks. (B) Total-field magnetic anomaly map of Vulcano
561 Island.



562
563
564
565
566
567

Figure 2 - (A) Map of the local residual anomalies produced by subtracting the 3D regional trend on the upward continued field. (B) Computed magnetic anomaly map. (C) Residual, total-field magnetic anomaly map produced by subtracting the computed field from the observed field.

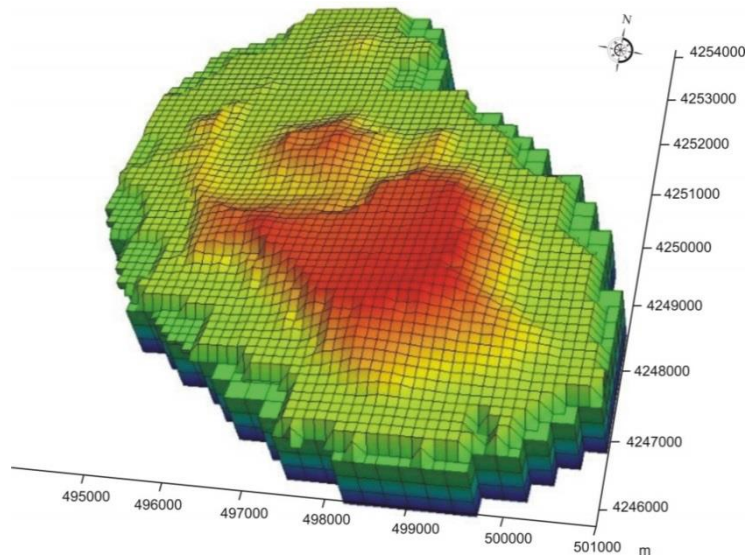
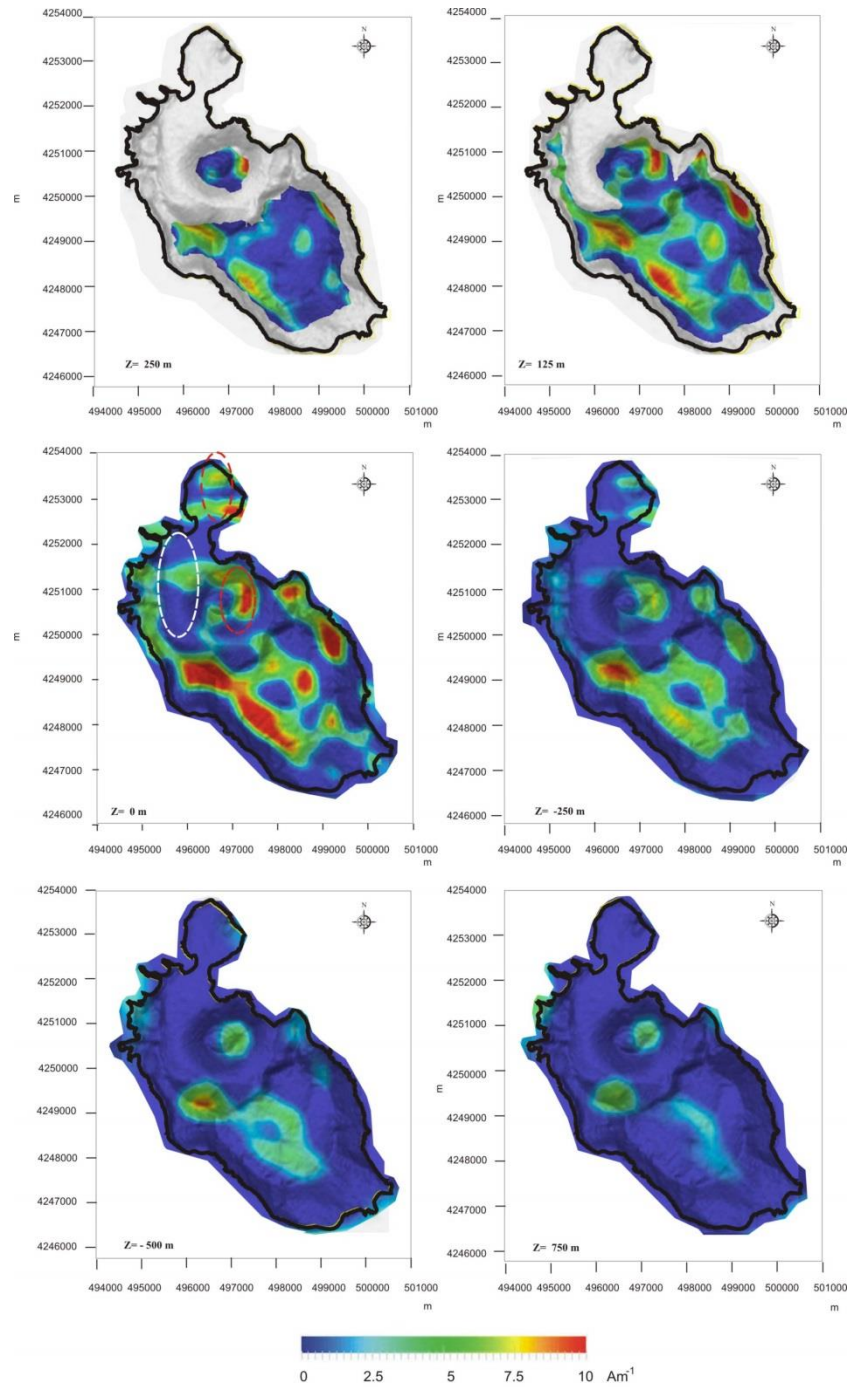
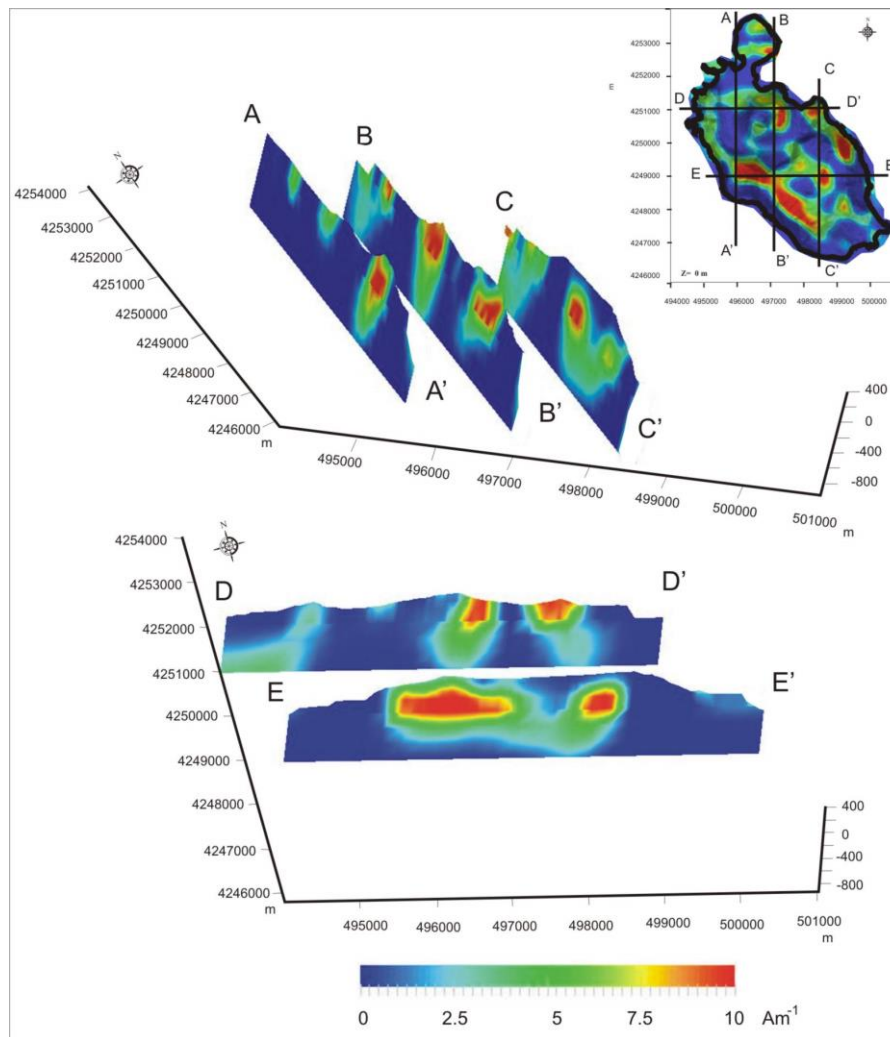


Figure 3 - Schematic configuration of the synthetic model used for the inversion process.



575
 576 Figure 4 - The 3D magnetization model of the Vulcano complex. Horizontal layers of the model
 577 from 250 above sea level to 750 m below sea level. The dashed areas, in the layer at 0 km of depth,
 578 represent the low (white ellipse) and high (red ellipses) Vp seismic anomalies detected by
 579 Chiarabba et al., (2004).

580
 581
 Corresponding author, e-mail address: rosalba.napoli@ingv.it (R. Napoli)



582

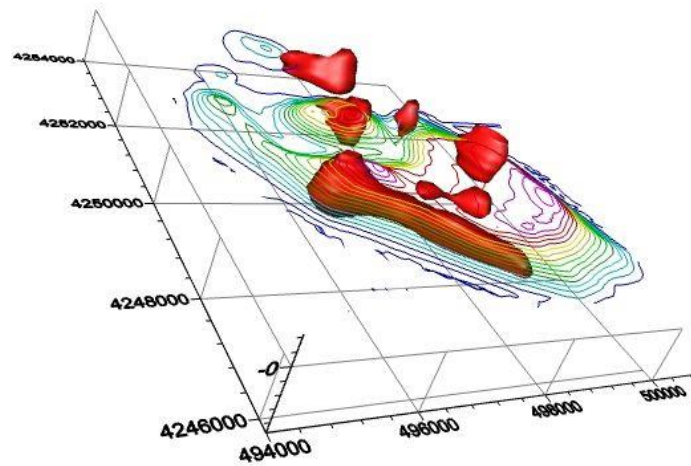
583

584 Figure 5 – North South and West-East vertical sections of the 3D magnetization model of the
 585 Vulcano complex. The inset shows the location of each profile superimposed to the horizontal layer
 586 at 0 km depth.

587

588

589



590
 591 Fig.6 – Three-dimensional volumes of the high-magnetization (more than 6 Am^{-1}) regions of the
 592 Vulcano complex.
 593